# Near Infrared Laser-Induced Targeted Cancer Therapy Using Thermoresponsive Polymer Encapsulated Gold Nanorods

Zhenjiang Zhang,[†] Jing Wang,[†] Xin Nie,[†] Tao Wen, Yinglu Ji, Xiaochun Wu, Yuliang Zhao, and Chunying Chen*

CAS Key Laboratory for Biomedical Effects of Nanomaterials and Nanosafety, National Center for Nanoscience and Technology of China, Beijing 100190, People's Republic of China

Ⓢ *Supporting Information*

ABSTRACT: External stimuli, such as ultrasound, magnetic field, and light, can be applied to activate in vivo tumor targeting. Herein, we fabricated polymer encapsulated gold nanorods to couple the photothermal properties of gold nanorods and the thermo- and pH-responsive properties of polymers in a single nanocomposite. The activation mechanism was thus transformed from heat to near-infrared (NIR) laser, which can be more easily controlled. Doxorubicin, a clinical anticancer drug, can be loaded into the nanocomposite through electrostatic interactions with high loading content up to 24%. The nanocomposite's accumulation in tumor post

systematic administration can be significantly enhanced by NIR laser irradiation, providing a prerequisite for their therapeutic application which almost completely inhibited tumor growth and lung metastasis. Since laser can be manipulated very precisely and flexibly, the nanocomposite provides an ideally versatile platform to simultaneously deliver heat and anticancer drugs in a laser-activation mechanism with facile control of the area, time, and dosage. The NIR laser-induced targeted cancer thermo-chemotherapy without using targeting ligands represents a novel targeted anticancer strategy with facile control and practical efficacy.
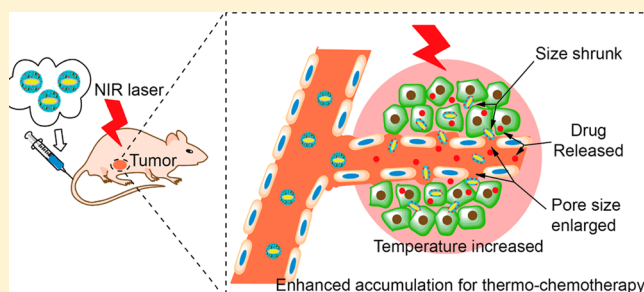
■ INTRODUCTION

Owing to their remarkable physicochemical properties, the application of nanomaterials to medicine offers potential solutions for many of the current challenges in cancer treatments. Integration of different materials into nanocomposites with each component acting in a coordinated way provides even more creative possibilities.[1−4] One such particular direction in nanomedicine is the development of so-called "theranostic" nanoplatforms, in which multiple nanocomponents with diagnostic and therapeutic functions are integrated into a single nanoplatform to realize the two functions simultaneously.[5,6] Another newly emerged direction to explore nanomedicine for cancer treatment is photothermal inorganic nanoparticles mediated thermo-chemotherapy.[7] These photothermal nanoparticles such as gold nanoparticles, have a high-absorption cross section for conversion of near-infrared (NIR) light to heat, and have been intensively explored for local hyperthermia and drug delivery. Nanoplatforms based on them have been developed for simultaneous delivery of heat and chemotherapeutic agents to tumor for thermo-chemo-therapy.[8]

Due to their tunable surface plasmon and photothermal effects, gold nanorods (AuNRs) have proven to be promising in a wide range of biomedical applications and ideally suited for theranostic and thermo-chemotherapeutic applications.[9−13] Effective accumulation of nanoparticles in tumors is crucial

for nanoparticle-mediated cancer diagnosis and treatment. To enhance their preferable accumulation, the surface of AuNR-based nanoplatforms is often modified with cell-specific ligands for active tumor targeting through receptor-mediated endocytosis pathways.[14] However, the in vivo performance of many ligand-modified tumor-targeted nanoparticles is not as good as initially envisioned because ligand attachment does not alter their biodistribution, and often decreases their blood circulation time and ligand affinity to its receptors.[15] External stimuli such as ultrasound and magnetic field have also been applied to activate in vivo tumor targeting.[16,17] Locally applied external heating can also induce site-specific accumulation of intravenously injected thermal-responsive polymers and their payloads.[15] These novel tumor-targeting strategies could be very efficient to enhance the selectivity of certain effects since the timing and intensity of the stimuli can be precisely controlled.

We have previously developed mesoporous silica coated AuNRs (Au@SiO$_2$) as an NIR laser mediated multifunctional theranostic nanoplatform for simultaneous drug delivery, hyperthermia therapy, and imaging in cancer cell lines.[16] Herein, we fabricated a nanocomposite by further coating Au@SiO$_2$ with a thermo- and pH-responsive polymer shell, poly(N-

Scheme 1. Nanocomposite Formulation Process (A) and NIR Laser Induced Targeted Thermo-Chemotherapy Using the Nanocomposite (B)
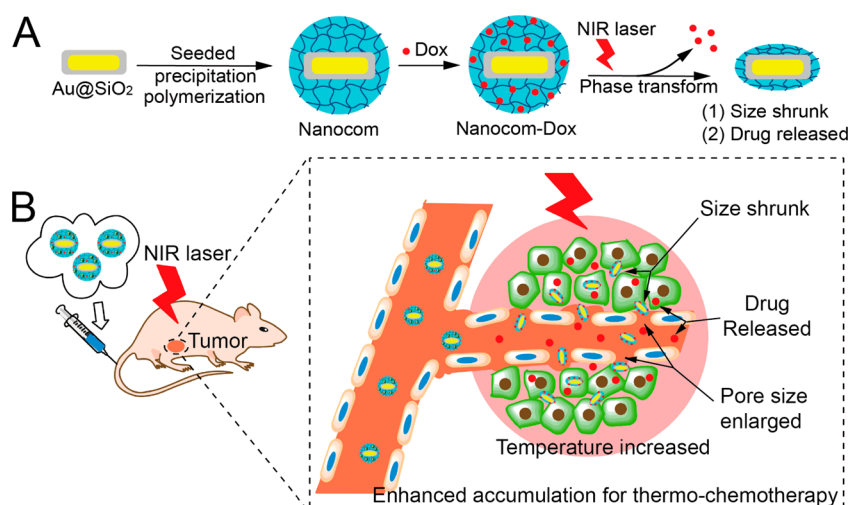
isopropylacrylamide-*co*-acrylic acid) and explored its in vivo applications. NIR laser irradiation at the tumor site following its intravenous administration to mice tumor models significantly enhanced their accumulation in tumor, providing a prerequisite for efficient cancer treatment which almost completely inhibited tumor growth (Scheme 1).

■ EXPERIMENTAL SECTION

Chemicals and Materials. All the chemicals and materials used were commercially available unless otherwise stated and were used without further purification. Deionized water (Millipore Milli-Q grade) with resistivity of 18.2 MΩ was used in all the experiments.

Instrumentation. Electron microscopy images were acquired on a FEI Tecnai G2 F20 U-TWIN transmission electron microscope (FEI Company, U.S.A.). UV−vis-NIR spectra and fluorescence spectra were obtained using a Tecan Infinite M200 spectrophotometer (Tecan Group, Switzerland). Zeta-potential measurements of the nano-particles were taken using a Malvern Zeta sizer Nano ZS instrument (Malvern Instruments, U.K.). A femtosecond laser beam (760 nm, 2 mm, 500 mW, 16 W/cm^2) was produced with a Ti:sapphire laser system (Spectra-Physics, Germany). A continuous wave laser (808 nm, 5 mm, 800 mW, 4 W/cm^2) was produced with a GCSLS-05−7W00 fiber-coupled diode laser system (Daheng Science&Technology, China). In vivo and ex vivo fluorescence microscopy was conducted using a Maestro 2 multispectral small-animal imaging system (Cambridge Research & Instrumentation, U.S.A.). The thermographs were measured by a Flir E40 compact infrared (IR) thermal imaging camera (FLIR Systems, U.S.A.). The amount of Au in samples was measured by an Elan DRC II inductively coupled plasma mass spectrometry (ICP-MS, PerkinElmer, U.S.A.). Serum biochemical analysis was performed using a biochemical autoanalyzer (Hitachi 7170, Japan). The pathological sections were observed by an optical microscope (Nikon U−III Multipoint Sensor System, U.S.A.).

Preparation and Stability Measurement of the Nano-composite. First, 1.25 μL 3-(Methacryloxy) propyl triethoxysilane (MPS) dissolved in 100 μL methanol was added to 10 mL Au@SiO$_2$ solution (0.5 nM nanoparticles), and the mixture was stirred for at least 4 h. Then the resulting solution of MPS-modified Au@SiO$_2$ was centrifuged to remove the unreacted MPS and resuspended in 2.5 mL water. In a typical procedure, an aqueous solution of 6.0 mL 100 mM *N*-isopropylacrylamide (NIPAM), 0.67 mL 100 mM acrylic acids, 1.2 mL 50 mM *N,N′*-methylenebis(acrylamide) (MBA), 100 μL 100 mM sodium dodecyl sulfate (SDS) and the above 2.5 mL MPS-modified Au@SiO$_2$ was added to a flask. The mixture was heated to 70 °C and bubbled through nitrogen for 0.5 h to remove residual oxygen. Then 1.0 mL 10 mM potassium persulfate (KPS) solution was rapidly

added, and the polymerization was allowed to proceed for an additional 4 h at 70 °C. Finally, the nanocomposites were collected by centrifugation and washed with water and methanol to remove the unreacted monomers. Different polymer thicknesses were obtained by varying the recipes of reactants. The stability of the nanocomposites at 37 °C were measured by UV−vis-NIR spectra for 2 weeks in water, 0.01 M phosphate buffer saline (PBS, pH = 7.4), and 100% fetal bovine serum, respectively (Supporting Information, SI, Figure S1)

Simulation Experiment of Increased Extravasation with Decreased Size. The nanocomposite solutions (1.74 mg/mL, Au content: 66 μg/mL) were first incubated in 25 °C, 37 °C, and 45 °C water bath for 15 min, respectively. Then, they were filtrated through the syringe filters with 0.22, 0.45, and 1 μm pore sizes, respectively. The filtrates were measured by UV−vis-NIR spectra and quantified by ICP-MS measurement of Au content. The filtrating efficiency equals the concentration of Au in filtrates/concentration of Au in initial solution.

Drug Loading and in Vitro Release. Dox was loaded to the nanocomposite by mixing 0.5 mL 1.2 mg/mL Dox solution in PBS buffer with 1 mL 1.74 mg/mL nanocomposite in PBS buffer for 12 h at room temperature. Then the dispersion was centrifuged (13 000 rpm, 8 min) to collect the Dox-loaded nanocomposite (Nanocom-Dox). The Dox concentration in the supernatant was determined by a UV−vis spectrophotometer at 480 nm to calculate the drug loading content. The drug loading content and entrapment efficiency were calculated by the following equations: Loading content = (weight of drug in Nanocom-Dox)/ (weight of A Nanocom-Dox); Entrapment efficiency = (weight of drug in Nanocom-Dox)/(initial weight of drug). Dox encapsulation efficiency was 92% and loading content reached up to 24%. A lower loading content of 3% was obtained by using a lower initial Dox 0.15 mg/mL. In the in vitro drug release experiment, 1.0 mL of Nanocom-Dox solution (1.7 mg/mL with Dox equivalent concentration of 317 μM) in different pH buffers (5.0 and 7.4) was agitated at 37 and 45 °C, respectively. The mixture was centrifuged at different time intervals. The supernatant was collected, and the same volume of fresh buffers was added back to the residual mixture. The amount of released drug in the supernatant was determined by measuring the absorption at 480 nm using a UV−vis spectrometer. The drug release profile in 100% fetal bovine serum was tested by fluorescence analysis with the excitation and emission wavelength set at 480 and 595 nm, respectively.

Cell Viability Assay. Murine breast carcinoma cell line 4T1 was maintained in RPMI 1640 medium (WISENT Inc., U.S.A.) supplemented with 10% fetal bovine serum (WISENT Inc., U.S.A.) and 1% penicillin-streptomycin (WISENT Inc.) at 37 °C in a humidified atmosphere of 5% CO$_2$. To determine the cytotoxicity, cells were plated in triplicate at a density of 2000 cells/well in 96-well

microplates (Costar, Corning, NY, U.S.A.). After incubation for 12 h, cells were exposed to 0.1, 1, 5, 10 μM of either Dox or equivalent dose of Nanocom-Dox or nanocomposite alone. Cytotoxicity was assessed at 12, 24, 48, and 72 h post treatment with a standard CCK-8 method.

Cellular Uptake of Dox. Intracellular uptake of Dox was quantified with a flow cytometry method based on the spontaneous fluorescence property of Dox. In brief, 4T1 cells were seeded in a 6-well plate, incubated overnight, and exposed to 5 μM Dox or equivalent dose of Nanocom-Dox for 24 h. After trypsinization, cells were washed three times with cold PBS and resuspended in HBSS. Cellular uptake of Dox was then determined by relative fluorescence intensity with excitation at 488 nm and emission at 560 nm.

Intracellular Localization Study. Fluorescence of Dox and lysosome (labeled by LysoTracker) was monitored to investigate the intracellular delivery of Dox by using a laser confocal scanning microscope (Ultra VIEW VoX, PerkinElmer U.S.A.). Briefly, 4T1 cells preseeded on Petri-dishes were incubated with RPMI1640 containing 5 μM Dox or equivalent dose of Nanocom-Dox. At 4 h post treatment, cells were rinsed twice with PBS and stained by Lysotracker Red DND-99 (Invitrogen, Carlsbad, California, U.S.A.) for 45 min. After rinsing with PBS, photographs of cells were obtained immediately by confocal microscope. The excitation wavelengths were 488 nm/563 nm for Dox/Lysotracker Red DND-99.

Blood Circulation Time of the Nanocomposite. To investigate blood circulation time of BSA-coated AuNRs, Au@SiO$_2$ and the nanocomposite, 200 μL suspensions with Au content of 66 μg/mL was intravenously injected in male balb/c mice (20 g body weight) from the tail. Blood samples were collected at 3 min, 10 min, 1 h, 2 h, and 24 h post administration, and stored at −20 °C before ICP-MS analysis.

Tumor Accumulation of the Nanocomposite-Dox in Vivo Mediated by Water Bath. Tumor bearing mice were prepared by implanting 1×10^6 murine 4T1 breast cancer cells at right hind leg in male balb/c mice. After the tumors had developed to about 1000 mm^3, mice were anaesthetized and had their right hind leg bearing the tumor immersed in a water bath at 42 °C for 5 min to preheat (the other part of the mouse body was thermally isolated from water bath). Dox, either loaded in the nanocomposite or in its free state, was intravenously injected and allowed for another 30 min of water bath to achieve the accumulation of Dox in the tumor (or no water bath as negative control). Then the mice were sacrificed and dissected tumor/spleen were imaged ex vivo to compare the accumulation of Dox in organs, utilizing a Maestro 2 in vivo imaging system with filters set at 500 nm/500−700 nm as the excitation/emission wavelength.

Tumor Accumulation of the Nanocomposite-IR820 in Vivo Mediated by Water Bath. Mice were similarly treated as above. IR820 (IR820 or equivalent IR820 concentration: 2 mg/kg body weight) instead of Dox, either loaded in the nanocomposite or in its free state, was intravenously injected and followed by 30 min of heating in water bath to achieve tumor accumulation. Then living mice were screened in a series of time points to monitor the dynamic variation of the nanocomposite accumulated in the tumor, with filters set at 690 nm/700−900 nm as excitation/emission wavelength. At the end point, mice were sacrificed and dissected organs were imaged in ex vivo.

Tumor Accumulation and Tissue Distribution of the Nanocomposite in Vivo Mediated by Laser Irradiation. Tumor bearing balb/c mice were prepared by implanting 1×10^6 murine 4T1 breast cancer cells at right hind leg. When the tumors reached about 100 mm^3 (approximately 0.1 g), mice were anaesthetized and were given a systemic injection of nanocomposite with equivalent Au content at 9.5 mg/kg body weight. Then a femtosecond laser irradiation at tumor site (or not for negative control) was immediately applied for 20 min to achieve accumulation (laser irradiation conditions: 760 nm, 500 mW, 16 W/cm^2). This dose is the same as the following in vivo tumor inhibition experiments, unless not otherwise stated. Mice were sacrificed at 30 min and 24 h post systemic injection of nanocomposite. Tumors and other organs were dissected and stored at −80 °C before ICP-MS analysis of Au element to evaluate the thermal-guided accumulation of the

nanocomposite. PEG modified Au@SiO$_2$ was used in accumulation study as a nonthermoresponsive control with same AuNR content injection dose and under same laser irradiation as above. The tumor tissues were collected at 30 min and 24 h post systemic injection.

Tumor Accumulation Dependence on the Size of Nanocomposite. Two nanocomposites with different polymer thicknesses (∼280 nm and ∼180 nm in diameter) were synthesized and respectively injected (1.32 mg Au/kg body weight) to 4T1 breast tumor (150 mm^3, ∼ 0.2 g) bearing mice without laser irradiation. Their accumulation was determined and compared at 24 h post injection by measuring the Au element using ICP-MS in tumor tissue.

ICP-MS for Au Element Quantification. For ICP-MS experiments, the above samples were predigested overnight with 4.0 mL concentrated HNO$_3$, then mixed with 3.0 mL 30% H$_2$O$_2$ and digested for 2 h in open vessels on a hot plate at 150 °C. When the residual volume decreased to ∼1 mL, 2.5 mL aqua regia was added to continue the digestion until the solution volume decreased to 0.5 mL. At last, the remaining solution was cooled and diluted to 3.0 g with a mixed acid solution containing 2% HNO$_3$ and 1% HCl. For quantitative analysis, a series of Au standard solutions (0.5, 1, 5, 10, 50, and 100 ppb) were prepared with the mixed acid solution and tested to obtain the standard curve. Bismuth (10 ppb) in the mixed acid solution was used as an internal standard solution. The amount of Au in samples was measured by an Elan DRC II ICP-MS (PerkinElmer, Waltham, MA, U.S.A.). Quantification was carried out by external six-point calibration with internal standard correction. Both the standard and the test solutions were measured three times by ICP-MS. The amount of Au was finally expressed as the percentage of the injected dose or normalized to the tissue weight per gram.

Therapeutic Evaluation of Nanocom-Dox in Tumor Bearing Mice. Tumor-bearing mice were prepared by implanting 1×10^6 4T1 cells at the right hind leg in male balb/c mice (20 g body weight). Two independent therapeutic experiments were conducted, taking intratumoral and tail vein injection as administration route, respectively. PBS, Dox (1 mg/mL), nanocomposite (25 mg/mL, Au content at 950 μg/mL, i.e., 9.5 mg Au/kg body weight) and Nanocom-Dox (25 mg/mL, with equivalent Dox concentration at 1 mg/mL and Au content at 950 μg/mL) were freshly prepared before use. For systemic injection experiments, a 200 μL of each above-mentioned solution was administered through the tail vein. For intratumoral injection experiments, a 50 μL solution was injected directly into and around the tumor, both at 4 days post inoculation, when the tumor volumes reached 40 mm^3 in average. For each of the two experiments, the tumors of half of the above four sets of mice were irradiated by NIR laser (760 nm, 500 mW, 16 W/cm^2) for 20 min, while the other half were left as unirradiated controls. Temperature change in tumor region under laser irradiation was recorded by an IR camera for the different groups. Tumor growth was monitored the following 10 days, and mice were sacrificed at 14 days post inoculation, tumors were dissected and weighed to evaluate the therapeutic efficacy of the different groups. The serum samples and different tissues were collected for the biochemical analysis and histopathological examination.

Synergistic Thermo-Chemotherapy of the Dox Loaded Thermoresponsive Nanocomposite with Laser Irradiation. Balb/c nude mice were implanted with 1×10^6 murine 4T1 breast cancer cells at the back. When the tumors reached about 60 mm^3, mice were anaesthetized and given a systemic injection of 200 μL PBS, nanocomposite (25 mg/mL, Au content at 950 μg/mL, i.e., 9.5 mg Au/kg body weight), or Nanocom-Dox (25 mg/mL, with equivalent Dox concentration at 1 mg/mL and Au content at 950 μg/mL). The nanocomposite and Nanocom-Dox groups were irradiated by an 808 nm continuous wave laser for 10 min. Different laser powers were used to control the highest tumor temperature to be 45 °C, 50 °C, or 58 °C, respectively. Temperature change in tumor region under laser irradiation was monitored by an IR camera. Tumor growth was monitored the following 10 days, and mice were sacrificed at 14 days post inoculation. Tumors were dissected and weighed to evaluate the therapeutic efficacy of different groups.
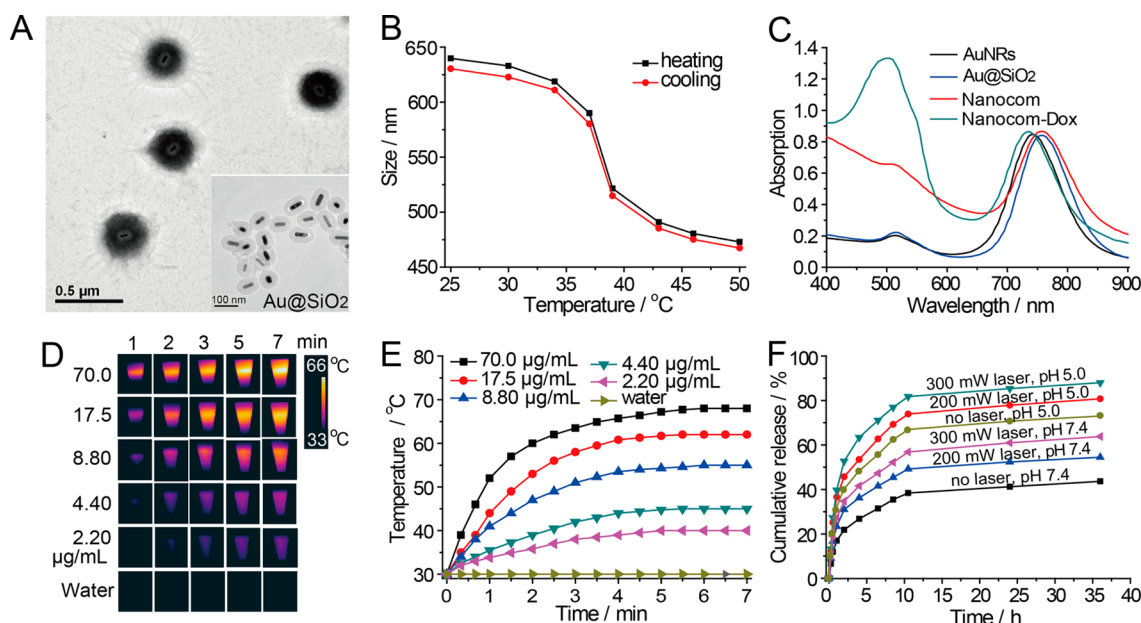
Figure 1. Characterization of the nanocompostie and laser-controlled drug release profiles. (A) TEM images of the nanocomposite and Au@SiO$_2$ (inset). (B) Reversible hydrodynamic size change of the nanocomposite with respect to temperatures. (C) Extinction spectra of AuNRs, Au@SiO$_2$, the nanocomposite (abbreviated as Nanocom in all figures), and Dox-loaded nanocomposite (abbreviated as Nanocom-Dox in all figures). (D) The temperature images of nanocomposite suspension under NIR laser (760 nm, 500 mW, 16 W/cm^2) irradiation were recorded by a IR camera at different concentration. (E) The rate of temperature rise and the final temperature were proportional to particle concentration at the constant laser function power (760 nm, 500 mW, 16 W/cm^2). (F) Dox release profiles from Nanocom-Dox with or without NIR laser irradiation at different pHs.

Serum Biochemical Analysis. Serum biochemical analysis was carried out using a standard protocol. After standing at room temperature for 3 h, the whole blood was centrifuged at 3000 rpm for 15 min. Then, serum was collected from the supernatant and examined by a biochemical autoanalyzer to explore the influence of Nanocom and Nanocom-Dox on liver function. Liver function was evaluated with serum levels of alanine aminotransferase (ALT), aspartate aminotransferase (AST), total bilirubin level (TBIL), total protein (TP), albumin (ALB), globulin (GLOB), alkaline phosphatase (ALP), and ALB/GLOB (A/G).

Histopathological Examination. The tissues (heart, liver, spleen, kidneys, and lung) were harvested and fixed in a 10% formalin solution. The histopathological tests were performed according to standard laboratory procedures. Tissue samples were numbered and given blind to the pathologist for conventional processing and analysis. Briefly, the tissue samples were embedded in paraffin blocks, sectioned into 5 μm slices, and mounted onto the glass slides. After hematoxylin-eosin (HE) staining, the sections were observed, and photos were taken using an optical microscope. (Magnification: liver ×10; heart, spleen, lung, and kidney ×20).

Statistical Analysis. Results are presented as mean or means ± standard deviation. One way analysis of variance was applied to evaluate the significance among groups according to Bonfferoni's post-test. $P < 0.05$ was considered to be statistically significant.

■ RESULTS AND DISCUSSION

Synthesis, Characterization and Thermoresponsive Properties of the Nanocomposite. Au@SiO$_2$ (inset of Figure 1A) was fabricated according to our previously reported protocol.[19,20] To couple photothermal properties and thermo-responsive properties in a single nanoplatform, a polymer layer consisting mainly of poly(N-isopropylacrylamide) (PNIPAM) was coated onto the surface of Au@SiO$_2$ by seeded precipitation polymerization.[21−23] PNIPAM is the most extensively studied thermoresponsive polymer which undergoes a reversible phase transition in aqueous solution from an extended hydrophilic chain to a condensed hydrophobic

globule when the temperature rises higher than 32 °C.[24] Acrylic acids were incorporated here to increase the phase transition temperature and for electrostatic absorption of positively charged drugs such as Dox. The nanocomposite has a well-defined core−shell structure of ∼280 nm diameter, and can be stably dispersed in solution with a temperature-independent (25−50 °C) zeta potential of −36 mV in water and −18.5 mV in pH 7.4 PBS (Figure 1A and SI Figure S1). The zeta potential is less negative at lower pHs due to the higher protonated acrylic acids content (SI Figure S2A). The polymer shell (P(NIPAM-AA)) is in a "doughnut" shape with loosely extending chains surrounded. The thickness of the "doughnut" part was optimized to be ∼70 nm for efficient drug loading by varying the ratio among the two monomers and cross-linkers (SI Figure S3). Dynamic laser scattering measurement showed that the nanoparticle size is both temperature- and pH-dependent, with a critical volume phase transition temperature at 39 °C in pH 7.4 PBS (Figure 1B and SI Figure S2B). At 45 °C, more than two times of nanocomposites can be extruded through a syringe filter with pore size of 450 nm than those at 25 and 37 °C (SI Figure S4). As the tumor leaky vessels have sizes of 100 nm to 2 μm, depending upon the tumor type, size decrease of nanoparticles at an elevated temperature should help their extravasation to tumor tissue.[25]

Drug Loading and Laser-Controlled Release. Dox was loaded into the nanocomposite through electrostatic interactions, forming a complex (abbreviated as Nanocom-Dox) with a loading content up to 24%. The longitudinal SPR peak after polymer coating and Dox loading remained in NIR region, which permits photons to penetrate biological tissues with relatively high transmissivity (Figure 1C).[26] Irradiated by NIR laser at its longitudinal SPR wavelength, the water suspension of the nanocomposite showed a rapid increase in temperature and eventually reached a plateau within 7 min (Figure 1D,E and SI Figure S5). The temperature rising rate and the final
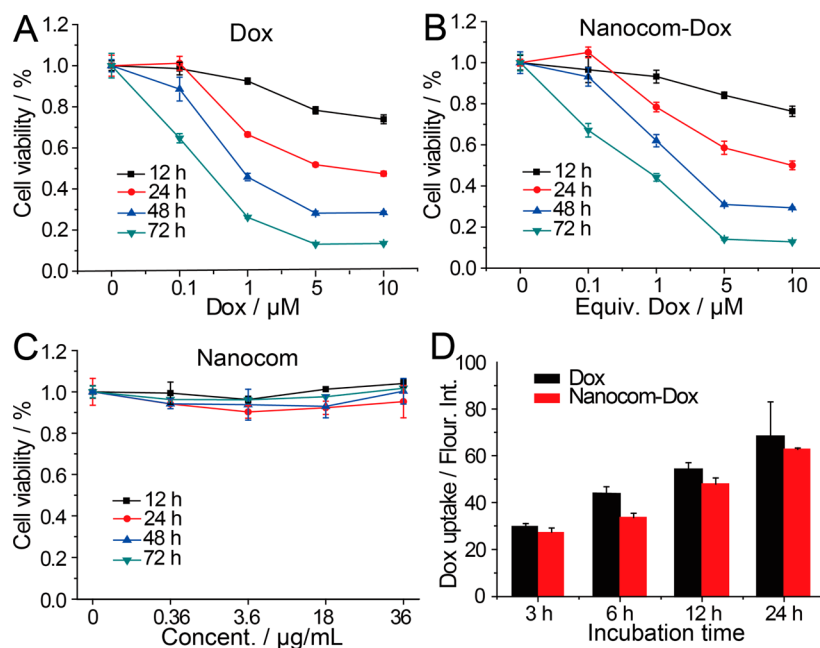
Figure 2. Cytotoxicity and cellular uptake of murine 4T1 breast cancer cells. Time- and dose-dependent effects of Dox (A), Nanocom-Dox (B), and nanocomposite (C) on the viability of murine 4T1 cells with equal concentrations of free dox, Nanocom-Dox, and Nanocom. (D) Cellular uptake of Dox and Nanocom-Dox quantified by flow cytometry. Murine 4T1 cells were exposed to 5 μM Dox or equivalent dose of Nanocom-Dox for 3, 6, 12, and 24 h.
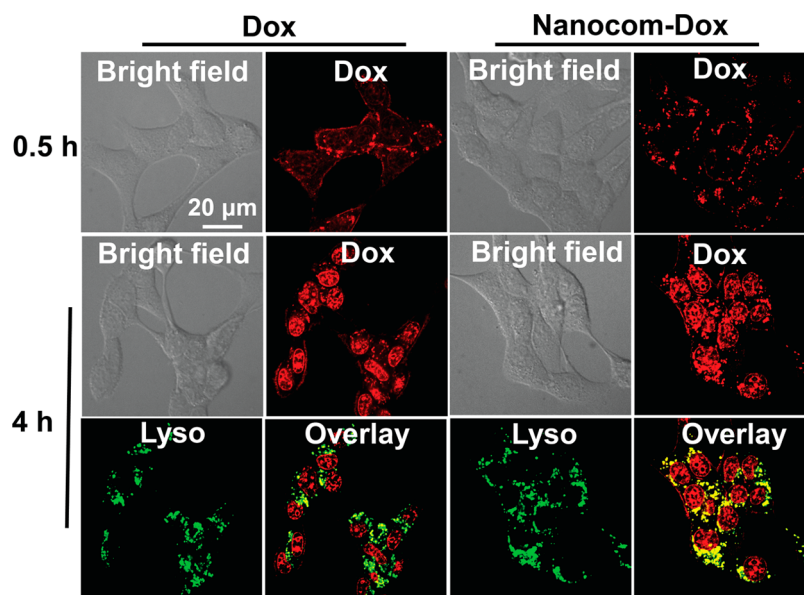

Figure 3. Inctracellular localization of Dox (red) and lysosome (green) in murine 4T1 breast cancer cells. The process of translocation of intracellular Dox was assessed using a laser confocal scanning microscope at 0.5h and 4 h post treatment of Dox and Nanocom-Dox with an equivalent dose of Dox at 5 μM.

temperature was proportional to the particle concentration and laser function power. The drug release rate can be significantly enhanced by laser irradiation at 200 or 300 mW, which heated the nanocomposite suspension up to 37 °C and 48 °C, respectively, because the laser-converted heat dissociated the electrostatic interactions between Dox and the polymer shell (Figure 1F). Dox release from Nanocom-Dox in 37 °C 100% fetal bovine serum 37 °C showed a similar profile with that in PBS buffer under 200 mW laser irradiation (SI Figure S6). Also observed was a pH-dependent release behavior with more Dox released at lower pHs.

Cell Viability, Uptake and Localization. The cytotoxicity of the nanocomposite was assessed using the standard protocol of cell counting kit-8 (CCK-8) assay. Free Dox and Nanocom-Dox with equivalent dose of Dox exhibited similar cytotoxic effect upon murine breast cancer 4T1 cells in a time and dose-dependent manner (Figure 2A,B), while the nanocompostie alone showed little cytotoxicity at a wide range of concentrations (Figure 2C).These results are quite reasonable since all the three components of the nanocomposites, AuNRs, mesoporous silica nanoparticles, and P(NIPAM-AA) hydrogels, have previously proven to be of low cytotoxicity and high
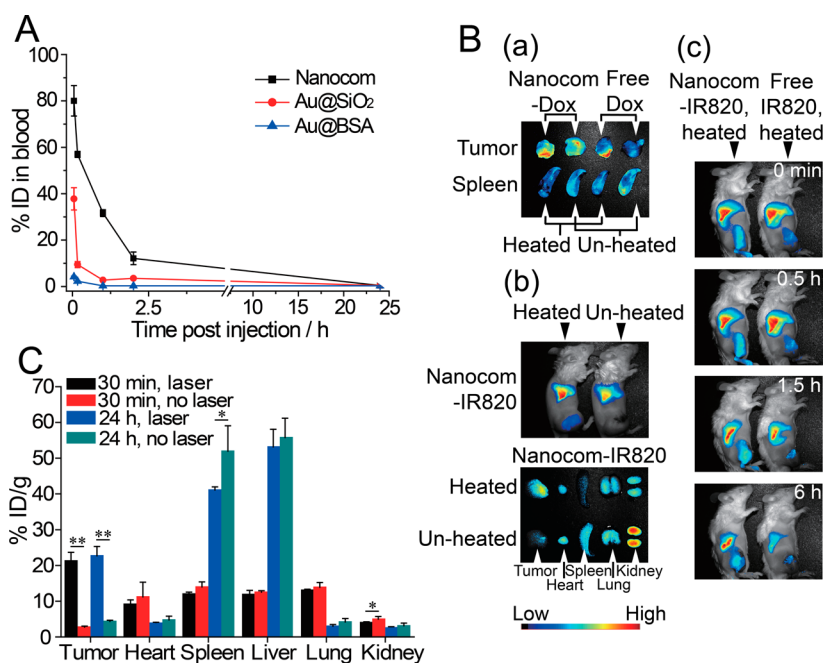
Figure 4. (A) Blood circulation time of Au@BSA, Au@SiO$_2$, and the nanocompostie analyzed by measuring Au content in blood by ICP-MS (data expressed as percentage of the injected dose (% ID)). (B) In vivo accumulation of the nanocomposite based on the fluororescent signals of Dox (a) or IR820 (b,c) compared with free Dox (a, right) or free IR820 (c, right) in a murine 4T1 breast cancer model. The mice were intravenously injected with the nanocomposite, followed by 30 min of heating the right hind leg bearing the tumor in a water bath at 42 °C (no water bath as negative control). The living mice were immediatly imaged (Bb) or were sacrificed, and the dissected organs were imaged in ex vivo (Ba). In order to compare with free IR820, the living mice were immediatly imaged or observed at 0.5 h, 1.5, and 6 h after 30 min water bath heating of the tumor following systemic administration, and the accumulation in tumor sustained more than 6 h after heating (Bc). (C) The biodistribution of the nanocomposite at 30 min and 24 h after systemic administration and NIR laser irradiation at the tumor based on ICP-MS anlysis (data expressed as percentage of the injected dose per gram of tissue (% ID/g). *$P < 0.05$ or **$P < 0.01$, significant difference between irradiated and unirradiated groups.

biocompatibility.[27−29] Flow cytometry results showed slightly lower cellular uptake of Dox in the case of Nanocom-Dox than that of free Dox within the first 24 h of incubation (Figure 2D). To further investigate the effects of nanocomposite formulation on intracellular localization of Dox, their intracellular local-ization in the living cells were observed by confocal microscopy (Figure 3). For cells treated with free doxorubicin, red fluorescence is visible inside cells suggesting fast diffusion and interlization as earlier as 0.5 h. Most Dox were observed in cellular nuclei after 4 h of incubation (Figure 3). After 4 h incubation, the Nanocom-Dox exhibit efficient intracellular delivery in tumor cells with colocalization in lysosome and partly entering into the nucleus, which suggests a time- and pH-dependent drug release profile within cells. The results confirm that the present nanocarrier can effectively deliver the drugs into living cells.

Blood Circulation. A long circulation time of nanoparticles in the bloodstream is often a prerequisite for successful targeted delivery and efficient treatment. On the basis of Au quantification by ICP-MS, the blood circulation time of the nanocomposite was significantly longer than that of Au@SiO$_2$ and the widely used bovine serum albumin coated AuNRs (Au@BSA) (Figure 4A). Indeed, the two latter nanoparticles were almost immediately (<10 min) cleared from the blood circulation after administration. The polymer shell may have helped to shield the particle surface and thereby reduce opsonization by blood proteins and phagocytosis by macro-phages.[30] Although its half-life might still not be sufficient for their effective accumulation in tumor, it opened a time window

for thermal operation in order to actively increase their accumulation in tumors.

Laser-Mediated Accumulation in Tumor. To evaluate their in vivo thermoresponsive properties, the accumulation of Nanocom-Dox in tumor tissues medicated by either water bath or NIR laser irradiation was evaluated through a murine 4T1 breast cancer model. First, Nanocom-Dox was intravenously injected through tail vein into 4T1 breast tumor bearing mice and the right hind leg bearing the tumor was immediately heated to 39−42 °C for 30 min by dipping it into a 42 °C water bath (SI Figure S7). Fluorescence signals of Dox of ex vivo tumors of the heated mice were significantly brighter than those of unheated mice, suggesting increased accumulation of Nanocom-Dox after heating (Figure 4Ba). Much more Dox was delivered to the tumor through Nanocom-Dox adminsitra-tion than that through direct administration of free Dox either before or after heating. To overcome the limited tissue penetration depth of Dox fluorescence at visible region, an NIR dye of IR820 was used instead of Dox for real-time visualization of their tumor accumulation. A significantly increased accumulation of Nanocom-IR820 was immediately observed after heating through in vivo imaging, and sustained for more than 6 h (Figure 4Bb,c). These results agreed with the literature about the tumor accumulation of thermoresponsive micelles with local heating treatment, suggesting that the nanocomposite also has an in vivo thermoresponsive behavior.[18]

Then, NIR laser was applied instead of water bath as external thermal stimuli to investigate tumor accumulation of the nanocomposite. The murine 4T1 breast tumor on the right
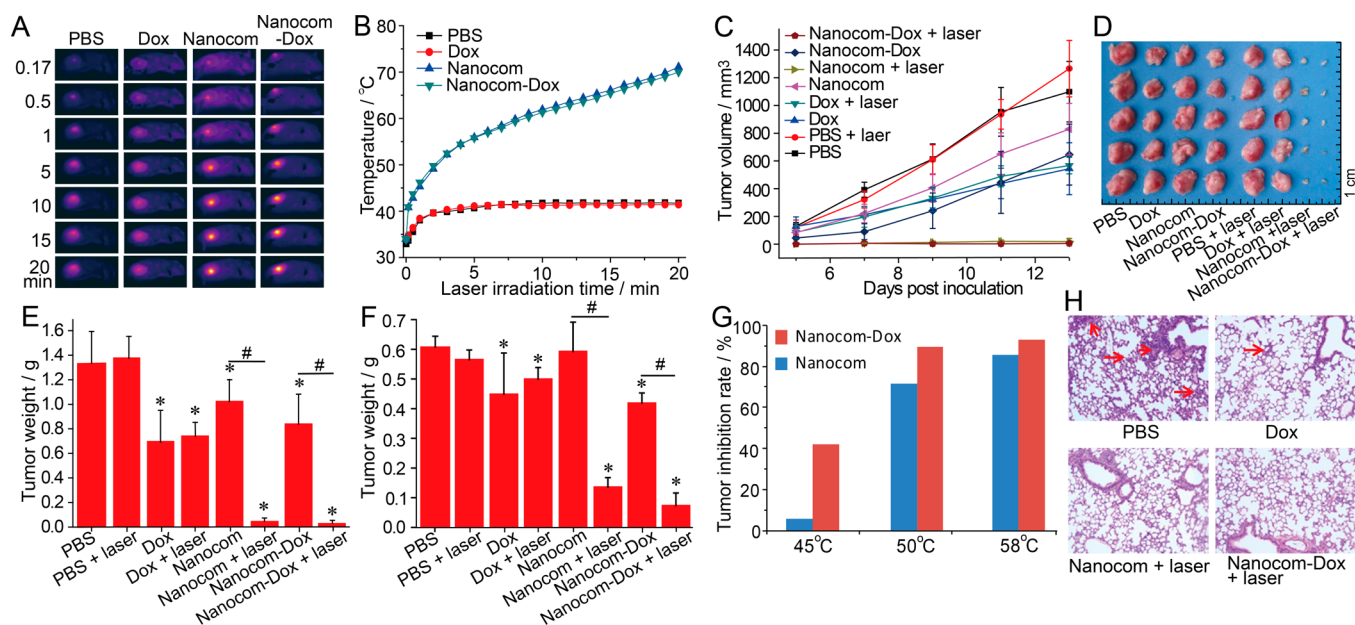
Figure 5. In vivo antitumor activity against murine 4T1 breast tumor after systematic administration or intratumoral injection. (A) The highest temperature within tumor region recorded by a IR camera after systematic administration and laser irradiation. (B) The heating curve of the four laser-irradiated groups. The antitumor activity including PBS, Dox, Nanocom, and Nanocom-Dox groups (with or without laser irradiation) through tail vein by measuring the tumor volume (C) and tumor weight (E). (D) Tumor dissection photographs through systematic administration. (F) The antitumor activity through intratumoral injection by measuring the tumor weight. (G) Tumor inhibition rate of the nanocomposite with and without Dox loaded under laser irradiation. Different laser power was used in three parallel experiments where the highest tumor surface temperature was recorded to be 45 °C, 50 °C, and 58 °C. (H) Hematoxylin—eosin (HE) staining of lung tissues after treatment and red arrows indicate the metastases. *$P < 0.05$, significant difference compared to unirradiated PBS group; #$P < 0.05$, significant difference between irradiated and unirradiated groups.

hind leg was very specifically irradiated by NIR laser for 20 min immediately following intravenous administration, and the tumor temperature increase was recorded using an IR camera at specific time intervals. Different from the above-discussed nanocomposite suspension, the irradiated tumor showed a rapid increase in temperature in the first minute and gradually changed to a slower and steady increase without eventually reaching a constant temperature within the irradiation time (Figure 5A). The highest temperature increase within the tumor region was typically ∼36 °C with an average temperature increase of the whole tumor estimated to be ∼20 °C (Figure 5B). The mice were then sacrificed, and the Au content in organs and tumor was measured by ICP-MS to quantify the nanocomposite accumulation (Figure 4C and SI Figure S8). At 30 min post injection, the laser-irradiated tumor showed a 7.6 times higher (1.45% of injected dose) accumulation of the nanocomposite than the unheated control, which sustained more than 24 h. NIR laser irradiation at the tumor site thus significantly increased the nanocomposite accumulation in tumor.

In order to understand the accumulation mechanism, the tumor accumulation of ∼180 nm (by TEM) nanocomposite and PEG coated Au@SiO$_2$ (Au@SiO$_2$−PEG) was compared with that of the above ∼280 nm nanocomposite. The smaller nanocomposite showed more than two times the accumulation of the larger one at 24 h post injection without laser irradiation, suggesting the tumor accumulation dependence on the size of the nanocomposite (SI Figure S9). The accumulation of Au@SiO$_2$−PEG at 30 min post injection increased 5.2 times with the same laser irradiation as above (SI Figure S10). We attribute this result to increased tumor vascular permeability at elevated temperatures, a well-established understanding in

tumor hyperthermia studies.[27] As a nonthermoresponsive control, the accumulation increase of Au@SiO$_2$−PEG with laser irradiation is less than the 7.6 times of the above ∼280 nm nanocomposite despite of their much smaller size (∼100 nm by TEM). This difference strongly suggests that the size of the nanocomposite decreased in vivo with laser irradiation due to their photothermal and thermoresponsive properties.

On the basis of the above observations, we proposed a mechanism to explain the NIR laser-induced tumor targeting using the nanocomposite. When the administered nanocomposites diffused in the bloodstream first flowed across the tumor vessels under laser irradiation, they converted the absorbed photon energy to heat, leading the tumor temperature to increase. The elevated tumor temperature, we hypothesize, caused two direct effects in vivo. The first one was to enlarge the pore size of the vasculature system within the tumor, which is supported by the well-established understanding that local hyperthermia can increase vascular permeability within tumors.[31] The second one was to shrink the size of the nanoparticles. Both of these effects would favor their extravasation from the vasculature system to the tumor tissue. With more nanocomposites flowing under the irradiation site, the tumor temperature was further increased due to a larger quantity of nanocomposites under laser irradiation. In turn, the further increased temperature strengthened the above two effects, leading more nanocomposites to accumulate in the tumor. This feedback loop cycle could explain the steady temperature increase of the tumor, rather than reaching a constant eventual temperature as the nanocomposite suspension did, due to a constant AuNRs quantity under irradiation. It is noted that there is no significant difference between the nanocomposites' tumor accumulation between 30 min and 24

h, although their concentration in blood was significantly decreased. The size of the nanocomposites should increase back to that at normal body temperature after the laser irradiation was stopped due to their reversible thermoresponsive property, which might block the tumor accumulated nanocomposites from going back to the vascular system.

It is worth mentioning that both water bath heating and NIR laser irradiation decreased the nanocomposite accumulation in the spleen, one of the major organs of the reticuloendothelial system (Figure 4Ba, Bb, and C). The retention in kidneys is also reduced, as shown by the ex vivo Dox and IR820 fluoresecence imaging and Au biodistribution results (Figures 4Bb and C).

Laser-Mediated Antitumor Activity. Since the nanocomposite accumulation in tumor can be significantly enhanced by NIR laser and the tumor temperature can be increased adequately for photothermal tumor ablation, we proceeded to evaluate their in vivo anticancer potentials. The nanocomposite with and without Dox, PBS, and free Dox were administered by a single intravenous injection to mice bearing murine 4T1 tumor (~40 mm^3). The tumors of half of the mice in each group were immediately irradiated with NIR laser for 20 min and compared with those of the other half as unheated controls. The irradiated Nanocom-Dox group showed a similar temperature rise curve with the above-discussed laser-irradiated nanocomposite alone group, and the tumors in the two groups of mice became whitish immediately after treatment, suggesting disruption of blood perfusion (Figure 5A,B). Remarkably, all these tumors regressed almost completely and became scar tissue within 14 days (SI Figure S11A). Comparatively, the PBS and Dox group only showed an increase of ~7 °C in the highest temperature of the tumor region and their temperature reached a plateau of 41.5 °C within 3 min. When the tumor volume of PBS group reached 1300 mm^3, all mice were sacrificed, and the tumor weight was measured (Figure 5C−E; SI Figures S11B−D). The two Dox groups showed a chemotherapeutic efficacy with a tumor inhibition rate ~47%, while the unirradiated Nanocom-Dox group ~38%, suggesting partial Dox was released in vivo without laser irradiation (Figure 5E). These results suggested that the photothermal effect of the nanocomposites alone was sufficient to inhibit tumor growth, while the Dox encapsulated by the nanocomposite could be released in vivo for chemotherapy after intravenous administration. In the laser-irradiated nanocomposite and Nanocom-Dox group, a similar temperature increase as above could be repeatedly achieved by irradiation at any time within the 14 days due to the sustained accumulation of nanocomposites in tumor (data not shown). These mice thus could be repeatedly treated whenever necessary.

We believe the enhanced accumulation of the nanocomposite induced by NIR laser was a prerequisite for their in vivo photothermal ablation efficacy. Provided that their accumulation in tumor had not been enhanced by NIR laser irradiation, more than 50% nanocomposites would be cleared from the blood at the end of a 20 min irradiation (Figure 3A). The left ones would not be sufficient to achieve the same temperature increase, which should be positively correlated with tumor growth inhibition rate. This hypothesis is supported by the limited temperature increase (average tumor temperature <45 °C) when the laser irradiation was postponed to 1 h after intravenous administration when ~70% of nanocomposite in blood was cleared or a lower dosage of 1/4 nanocomposite quantity was administered (data not shown).

In order to show in vivo the laser controlled drug release, i.e., efficacy of chemotherapy, more clearly, the growth inhibition ability of the nanocomposite with and without Dox under laser irradiation was compared in mice bearing murine 4T1 tumor (~60 mm^3). The two nanocomposites were intravenously injected, and the tumors were immediately irradiated with NIR laser for 10 min. In three parallel experiments, the laser function power was all lower than that used above to control the highest tumor temperature to be 45 °C, 50 and 58 °C, respectively. At all of the three temperatures, the tumor inhibition rate of Dox-loaded nanocomposite was significantly higher than that of nanocomposite alone, suggesting the efficacy of chemotherapy from Dox release (Figure 5G). With temperature rise, the hyperthermia efficacy of nanocomposite alone with laser reasonably increased while the difference of inhibition rate between the two groups decreased, suggesting inhibition was mainly due to chemotherapy at lower temperatures, such as 45 °C (in accord with the inhibition results of free Dox in Figure 5E) but due to hyperthermia at higher temperatures such as 58 °C.

The thermo-chemotherapy efficacy through intratumoral injection was also evaluated with the same regimen. Although the accumulated nanocomposites and Dox within and around the tumor (1/4 of the intravenous dose) were much more than those through intravenous injection (1.45%, SI Figure S8), the photothermal ablation efficacy of irradiated nanocomposite and Nanocom-Dox, and the chemotherapy efficacy of the two Dox groups and unirradiated Nanocom-Dox group was less efficient than their intravenously injected counterparts (Figure 5F and SI Figure S11). We attribute the better efficacy of intravenous administration to more efficient diffusion of the therapeutic agents within the whole tumors, which was extremely difficult to achieve through intratumoral injection due to the high intratumoral pressure. A synergistic efficacy in the irradiated Nanocom-Dox group, which was better than the photothermal ablation efficacy of the irradiated nanocomposite group and the chemotherapy efficacy of unirradiated Nanocom-Dox group was obseved as expected. Compared to the traditional thermo-chemotherapy, the nanoparticle-mediated counterpart ruled out the systemic side effects of chemotherapy and the challenges in hyperthermia operation with the same advantage of synergistic efficacy.[32]

To test the toxicity of the nanocomposites, liver function was evaluated with serum levels of ALT, AST, TBIL, TP, ALB, GLOB, and ALP (SI Table S1). The Nanocom+laser and Nanocom-Dox+laser groups have lower values of the [AST/ALT] compared to the saline and Dox groups, despite their highly efficient inhibition of tumor growth. The levels of total bilirubin, which is produced when liver breaks down old red blood cells, also decreased after all treatments. All of the toxicity data suggest that the tested nanocomposites did not cause liver dysfunction in mice within the treatment period.

Subsequently, the histopathological examinations of the tissues (heart, liver, spleen, lung, and kidneys) were performed by standard histological techniques with HE staining. The Nanocom+laser and Nanocom-Dox+laser groups showed neither obvious pathological changes in heart, spleen, and kidney, nor obvious liver damage. Local inflammatory response of lymphocytic infiltration in the liver sections indicated by the dense blue staining might be induced by the nanocomposite accumulation (SI Figure S12). Because the 4T1 cells are highly malignant tumor cells, obvious lung metastases (Figure 5H, red arrows indicate the metastases) were observed in the PBS

7324

dx.doi.org/10.1021/ja412735p | J. Am. Chem. Soc. 2014, 136, 7317−7326

group. The Dox group showed slight lung metastases, while the Nanocom+laser and Nanocom-Dox+laser groups did not show any metastases due to their highly efficient tumor inhibition, indicating the advantages of the nanocomposites for tumor therapy.

■ CONCLUSIONS

In summary, we successfully coupled photothermal properties and thermoresponsive properties in a single nanocomposite by coating Au@SiO$_2$ with a thermoresponsive polymer shell consisting mainly of PNIPAM. The activation stimulus was transformed from heat to NIR laser, which could be used to control its size as well as drug release. The nanocomposite showed minimal cytotoxicity and high biocompatibility in cell experiments. The thermoresponsive polymer shell helped prolong its blood circulation time. Both local water bath heating and NIR laser irradiation at the tumor region following intravenous administration could significantly increase their accumulation in tumor. The improved accumulation in tumor with NIR laser irradiation induced sufficient temperature increase that almost completely inhibited tumor growth, showing very promising potentials of the nanocomposite for tumor treatments. Since laser can be manipulated very precisely and flexibly, the nanocomposite provides an ideally versatile platform to simultaneously deliver heat and anticancer drugs in a laser-activation mechanism with facile control of the area, time, and dosage. The NIR laser irradiation-induced actively targeted cancer treatment without using active targeting ligands represents a novel targeted anticancer strategy with facile external control and practical efficacy. We anticipate that the present nanocomposite could be accommodated with different therapeutics, and could be similarly incorporated with other NIR responsive inorganic nanoparticles for the treatments of a myriad of human diseases.

■ ASSOCIATED CONTENT

Ⓢ Supporting Information

Figures S1−S12 and Table S1, including the stability of nanocomposites in pure water, PBS, and bovine serum; pH-dependent Zeta potential and size; simulation experiment data of increased extravasation with decreased size; Dox release profile from Dox loaded nanocomposite in fetal bovine serum; ICP-MS analysis of biodistribution of the nanocomposite after systemic administration and NIR laser irradiation at the tumor with data expressed as percentage of the injected dose (% ID); tumor accumulation dependence on the size of thermoresposive nanocomposite; the tumor accumulation of the nanocomposite and PEG coated Au@SiO$_2$ (Au@SiO$_2$−PEG) at 30 min and 24 h after systemic administration and NIR laser irradiation at the tumor; antitumor activity against murine 4T1 tumor after systematic administration or intratumoral injection; hematoxylin—eosin (HE) staining of tissues after treatment; and the influence of Nanocom and Nanocom-Dox on liver function after treatment using serum biochemical analysis. This material is available free of charge via the Internet at http://pubs.acs.org.

■ AUTHOR INFORMATION

Corresponding Author

chenchy@nanoctr.cn

Author Contributions

†These authors contributed equally.

Notes

The authors declare no competing financial interest.

■ REFERENCES

(1) Sailor, M. J.; Park, J. H. *Adv. Mater.* **2012**, *24*, 3779−3802.
(2) Park, J. H.; Maltzahn, G. V.; Ong, L.; Centrone, A.; Hatton, T. A.; Ruoslahti, E.; Bhatia, S. N.; Sailor, M. J. *Adv. Mater.* **2010**, *22*, 880−885.
(3) Park, J. H.; Maltzahn, G. V.; Xu, M. J.; Fogal, V.; Kotamraju, V. R.; Ruoslahti, E.; Bhatia, S. N.; Sailor, M. J. *Proc. Natl. Acad. Sci. U.S.A.* **2010**, *107*, 981−986.
(4) Maltzahn, G. V.; Park, J. H.; Lin, K. Y.; Singh, N.; Schwöppe, C.; Mesters, R.; Berdel, W. E.; Ruoslahti, E.; Sailor, M. J.; Bhatia, S. N. *Nat. Mater.* **2011**, *10*, 545−552.
(5) Lammers, T.; Aime, S.; Hennink, W. E.; Storm, G.; Kiessling, F. *Acc. Chem. Res.* **2011**, *44*, 1029−1038.
(6) Zhang, Z.; Wang, J.; Chen, C. *Theranostics* **2013**, *3*, 223−238.
(7) Melancon, M. P.; Zhou, M.; Li, C. *Acc. Chem. Res.* **2011**, *44*, 947−956.
(8) Zhang, Z.; Wang, J.; Chen, C. *Adv. Mater.* **2013**, *25*, 3869−3880.
(9) Wang, L.; Li, Y. F.; Zhou, L.; Liu, Y.; Meng, L.; Zhang, K.; Wu, X.; Zhang, L.; Li, B.; Chen, C. *Anal. Bioanal. Chem.* **2010**, *396*, 1105−1114.
(10) Qiu, Y.; Liu, Y.; Wang, L.; Xu, L.; Bai, R.; Ji, Y.; Wu, X.; Zhao, Y.; Li, Y.; Chen, C. *Biomaterials* **2010**, *31*, 7606−7619.
(11) Chen, H.; Shao, L.; Li, Q.; Wang, J. *Chem. Soc. Rev.* **2013**, *42*, 2679−2724.
(12) Wang, L.; Liu, Y.; Li, W.; Jiang, X.; Ji, Y.; Wu, X.; Xu, L.; Qiu, Y.; Zhao, K.; Wei, T.; Li, Y.; Zhao, Y.; Chen, C. *Nano Lett.* **2011**, *11*, 772−780.
(13) Xu, L.; Liu, Y.; Chen, Z.; Li, W.; Wang, L.; Wu, X.; Ji, Y.; Zhao, Y.; Ma, L.; Shao, Y.; Chen, C. *Nano Lett.* **2012**, *12*, 2003−2012.
(14) Basile, L.; Pignatello, R.; Passirani, C. *Curr. Drug Targets* **2012**, *9*, 255−268.
(15) Chen Weihsu, C.; Zhang Andrew, X.; Li, S.-D. *Eur. J. Nanomed.* **2012**, *4*, 89−93.
(16) Veiseh, O.; Gunn, J. W.; Zhang, M. *Adv. Drug Delivery Rev.* **2010**, *62*, 284−304.
(17) Schroeder, A.; Kost, J.; Barenholz, Y. *Chem. Phys. Lipids* **2009**, *162*, 1−16.
(18) Chilkoti, A.; Dreher, M. R.; Meyer, D. E.; Raucher, D. *Adv. Drug Delivery Rev.* **2002**, *54*, 613−630.
(19) Zhang, Z.; Wang, L.; Wang, J.; Jiang, X.; Li, X.; Hu, Z.; Ji, Y.; Wu, X.; Chen, C. *Adv. Mater.* **2012**, *24*, 1418−1423.
(20) Gorelikov, I.; Matsuura, N. *Nano Lett.* **2007**, *8*, 369−373.
(21) Kawano, T.; Niidome, Y.; Mori, T.; Katayama, Y.; Niidome, T. *Bioconjugate Chem.* **2009**, *20*, 209−212.
(22) Shiotani, A.; Akiyama, Y.; Kawano, T.; Niidome, Y.; Mori, T.; Katayama, Y.; Niidome, T. *Bioconjugate Chem.* **2010**, *21*, 2049−2054.
(23) Tang, H.; Shen, S.; Guo, J.; Chang, B.; Jiang, X.; Yang, W. *J. Mater.Chem.* **2012**, *22*, 16095−16103.
(24) Rapoport, N. *Prog. Polym. Sci.* **2007**, *32*, 962−990.
(25) Hobbs, S. K.; Monsky, W. L.; Yuan, F.; Roberts, W. G.; Griffith, L.; Torchilin, V. P.; Jain, R. K. *Proc. Natl. Acad. Sci. U.S.A.* **1998**, *95*, 4607−4612.
(26) Weissleder, R. *Nat. Biotechnol.* **2001**, *19*, 316−317.
(27) Vihola, H.; Laukkanen, A.; Valtola, L.; Tenhu, H.; Hirvonen, J. *Biomaterials* **2005**, *26*, 3055−3064.
(28) Asefa, T.; Tao, Z. *Chem. Res. Toxicol.* **2012**, *25*, 2265−2284.

(29) Wang, L.; Jiang, X.; Ji, Y.; Bai, R.; Zhao, Y.; Wu, X.; Chen, C. *Nanoscale* **2013**, *5*, 8384−8391.

(30) Koo, H.; Huh, M. S.; Sun, I. C.; Yuk, S. H.; Choi, K.; Kim, K.; Kwon, I. C. *Acc. Chem. Res.* **2011**, *44*, 1018−1028.

(31) Chatterjee, D. K.; Diagaradjane, P.; Krishnan, S. *Ther. Delivery* **2011**, *2*, 1001−1014.

(32) Hauck, T. S.; Jennings, T. L.; Yatsenko, T.; Kumaradas, J. C.; Chan, W. C. W. *Adv. Mater.* **2008**, *20*, 3832−3838.